Journal of Zhejiang University-SCIENCE A (Applied Physics & Engineering) in press
www.jzus.zju.edu.cn; www.springer.com/journal/11582
E-mail: jzus_a@zju.edu.cn

Research Article

https://doi.org/10.1631/jzus.A2300492

Investigation on the resilient modulus of soil mixture at various water contents and coarse grain contents under train moving loads

Yu SU[1,2], Yue ZHANG[1], Junyi DUAN[1]✉, Jianglin GAO[2], Zhongzheng WANG[3], Da LIU[2], Bo HAN[1], Wenzhe ZHU[1]

[1]*School of Infrastructure Engineering, Nanchang University, Nanchang 330031, China*
[2]*Jiangxi hydraulic safety engineering technology research center, Jiangxi Academy of Water Science and Engineering, Nanchang 330029, China*
[3]*School of Mechanical, Medical and Process Engineering, Faculty of Engineering, Queensland University of Technology, QLD 4001, Australia*

Abstract: Interlayer soil in railway substructures is characterized by a fine/coarse soil mixture. Considering that the resilient modulus M_r of the mixture is influenced by the microstructure of fine soil, it appears worthwhile to investigate this aspect further. In this work, the microstructure of fines was explored by mercury intrusion porosimetry, and its influence on the M_r of the mixture was studied by multi-stage dynamic triaxial tests with varying deviator stress amplitudes σ_d. The results showed a fine matrix fabric obtained at water contents of fine soil w_f=17.6% and 13.7% (> the plastic limit of fine soil w_p=12%), and a fine aggregate fabric identified at w_f=10.6% (< w_p=12%). Interestingly, the influences of w_f and σ_d on the M_r of the mixture were observed: the rise in σ_d contributed to a decline in M_r when $w_f>w_p$ but to an increase in M_r when $w_f<w_p$. It was concluded that, for the fine matrix fabric ($w_f>w_p$), increasing σ_d induced a reduction in M_r, while for the fine aggregate fabric ($w_f<w_p$), increasing σ_d gave rise to the growth of M_r. The distinct M_r–σ_d behaviors for these two fabrics were explained by the competing influences between soil hardening upon loading and soil rebounding upon unloading. For the fine matrix fabric ($w_f>w_p$), considering its high deformability, the rebounding effect on M_r outweighed the hardening effect, thus a decline in M_r occurred with the growth of σ_d. Conversely, for the fine aggregate fabric ($w_f<w_p$), the rebounding effect on M_r was secondary compared with the hardening effect based on the consideration of its low deformability, thus an increase in M_r was observed with rising σ_d.

Key words: Railway engineering; Resilient modulus; Unsaturated soil; Microstructure

1 Introduction

An interlayer in the railway substructure commonly forms owing to decades of train moving loads. In-situ observation shows that this interlayer soil consists of ballast grains and subgrade fines. With an increasing depth of the interlayer, the ballast grain content declines (Trinh, 2011). As a component of the railway substructure, the resilient modulus M_r of interlayer soil is a crucial parameter for the performance of rail tracks. With the ongoing demand for increased axle loads in railway transportation, the deviator stress amplitudes σ_d (determined by the subtraction between the maximum and the minimum deviator stresses for one loading cycle) increase, which facilitates the degradation of the ballast and thus causes a reduction in its resilient modulus M_r (Indraratna et al., 2021). On the other hand, the water level in the field varies frequently, which facilitates the variation in M_r of the soil mixture. To obtain a thorough understanding of M_r of the soil mixture, it is necessary to explore this parameter at distinct water contents and coarse grain contents under train moving loads.

The impact of water content on the M_r of railway subgrade soil was examined: under saturation, an accumulation of pore water pressure was induced by traffic loadings, which resulted in a decline in M_r. With a reduction in the water content, M_r increased because of the suction effect (Duong et al., 2013; Charles et al., 2019; Wang et al., 2019; Zheng et al., 2020; Wan et al., 2020; Bian et al., 2022; Hu and Bian, 2022). Lokkas et al. (2021) suggested that soil behavior is crucial for the infrastructure. Alamanis et al.

✉ Junyi DUAN, jyduan91@ncu.edu.cn
Junyi DUAN, https://orcid.org/0000-0002-1798-833x

Received Oct. 3, 2023; Revision accepted Dec. 26, 2023; Crosschecked

(2021) developed the assessment principles for the shear strength of clayey soil by experiments. Anagnostopoulos et al. (2020) explored the shear strength parameters of grouted coarse soil, and found that the injectability of cement grouts into coarse soil contributed to an increase in its cohesion. Sun et al. (2018) performed dynamic triaxial tests on railway ballast and reported that a large reduction of M_r occurred with an increasing coefficient of uniformity. Wang et al. (2017) carried out dynamic triaxial tests to address the influence of coarse grain content f_v on the M_r of the soil mixture. They identified a characteristic value $f_{v\text{-}cha}$; with an increase in f_v, a slow rising rate of M_r was observed when $f_v<f_{v\text{-}cha}$ while a fast rising rate of M_r occurred when $f_v>f_{v\text{-}cha}$. This was because the former was characterized by a fine soil-supported fabric, while the latter featured a coarse grain-supported fabric. Duong et al. (2016) addressed the influences of w and f_v on the M_r of the soil mixture. They reported that the growth of f_v facilitated the increase in M_r at saturation but a decline in M_r at unsaturation. It should be noted that in previous studies, a stable dry density of soil mixture ρ_d was controlled for the mixture with different f_v values. Under this circumstance, the dry density of fine soil fraction $\rho_{d\text{-}f}$ declined with an increase in f_v, which induced a reduction in suction. As a result, both f_v and suction changed, rendering the test results difficult to analyze.

Lekarp et al. (2000) reviewed the influence of various factors (e.g., confining pressure σ_3, deviator stress amplitude σ_d, etc.) on the M_r of unbound aggregates and found that σ_3 and σ_d played important roles. Sun et al. (2016) executed dynamic triaxial tests to address the effects of σ_3 and σ_d on the M_r of ballast and found that it rose with increasing σ_3 and σ_d. Ng et al. (2013) worked on the effect of σ_d on the M_r of subgrade soil, and indicated that an increase in σ_d induced a decline in M_r at a low suction ψ ranging from 0 to 250 kPa (the corresponding w ranged from 20.5% to 6.8%). Yang et al. (2008) explored the M_r of cohesive soil with various σ_d and ψ values: with the growth of σ_d, the M_r declined at low ψ=50 and 150 kPa (w=23.2% and 20.2%) but increased at high ψ=450 kPa (w=19.1%). Su et al. (2021a) executed dynamic triaxial tests to address the combined influences of σ_d and w on the M_r of mixture. In their study, an increase in σ_d induced a decline in M_r at high w=17.6% but an increase in M_r at low w=10.6%. However, these studies focused solely on the influences of traffic loading and w (or ψ) on the M_r of soil and failed to explore its microstructural mechanism, especially of the soil mixture. Notably, in this work, the M_r of soil was obtained by performing dynamic triaxial tests and microstructure observation was conducted by mercury intrusion porosimetry. Based on the results, it appears vital to explore the relationship between the M_r of the soil mixture and its microstructure.

The purpose of the present research was to identify the impacts of w, f_v and σ_d on the M_r of the soil mixture in the conventional railway substructure. Multi-stage dynamic triaxial tests were executed, allowing the determination of M_r under varying w, f_v and σ_d values. Mercury intrusion porosimetry was carried out to examine the influence of water contents of fine soil w_f on the microstructure of fine soil fraction. The results allowed us to shed light on the relationship between the variation in M_r and that in the microstructure.

2 Materials and methods

2.1 Reconstituted fine soil and micro-ballast

In our laboratory experiment, the intact interlayer soil was substituted by a mixture of reconstituted fines and micro-ballast. Fig. 1(a) compares the grain size distribution (GSD) curves of reconstituted fine soil and natural fine soils, which show good agreement. Note that the reconstituted fines consist of a small proportion of clay content (30%) and a large proportion of sand content (70%) (Wang et al. 2017). The soil properties of reconstituted fines were as follows: optimum water content $w_{opt\text{-}f}$=13.7% and maximum dry density $\rho_{dmax\text{-}f}$=1.82 Mg/m^3. Fig. 1(b) presents the GSD curves of ballast and micro-ballast (see more details in Qi et al. 2020a). In accordance with Qi et al. (2020b), the parameter of coarse grain content f_v was employed to describe the number of micro-ballast in the mixture (Section S1). The cohesion c and friction angle φ of fine/coarse soil mixture with varying f_v values were presented in Table 1, which were obtained from Su et al. (2020).

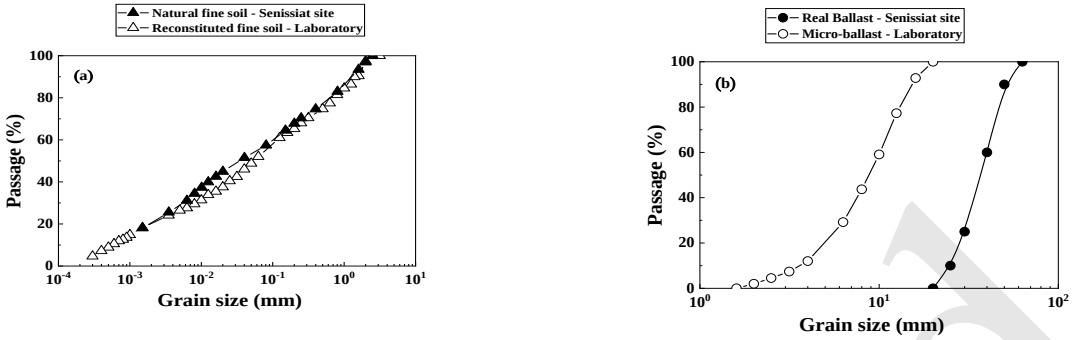

Fig. 1. Comparisons of GSD curves for (a) natural fine soil and reconstituted fine soil, and (b) real ballast and micro-ballast

Table 1. Soil properties of samples in cyclic triaxial tests

f_v (%)	Fine soil fraction			Soil mixture			Shear strength parameters	
	$w_{opt\text{-}f}$ (%)	Target w_f (%)	Target $\rho_{dmax\text{-}f}$ (Mg/m^3)	Target S_r (%)	Target ρ_d (Mg/m^3)	Measured ρ_d (Mg/m^3)	Cohesion c (kPa)	Friction angle φ (°)
0	13.7	17.6	1.82	100	1.82	1.80	32	8
		13.7		78		1.82	61	15
		10.6		60		1.85	137	21
10		17.6		100	1.91	1.88	32	9
		13.7		78		1.91	56	18
		10.6		60		1.93	129	27
20		17.6		100	1.99	1.97	29	12
		13.7		78		1.99	52	21
		10.6		60		2.01	125	27
35		17.6		100	2.12	2.11	27	22
		13.7		78		2.12	43	31
		10.6		60		2.13	102	38
45		17.6		100	2.21	2.20	26	34
		13.7		78		2.21	30	38
		10.6		60		2.22	98	46

In this study, a constant $\rho_{d\text{-}f}$ value (1.82 mg/m^3), three target w_f values (17.6%, 13.7% and 10.6%) and five target f_v values (0%, 10%, 20%, 35%, and 45%) were considered. Table 1 presents the detailed soil properties of the samples. For the experiment, fine soil was prepared at $w_{opt\text{-}f}$=13.7%, followed by storage in a sealed container with a duration of at least 24 h. A soil mixture with a target f_v value was obtained by mixing fine soil with coarse grains (Fig. 2(a)). This mixture was dynamically compacted to a cylindrical sample (Fig. 2(b)). Note that the $\rho_{d\text{-}f}$=1.82 Mg/m^3 of the fine soil was controlled to be the same for mixtures with varying f_v. With an increase in f_v, the dry density of mixture ρ_d also elevated.

The as-compacted sample at $w_{opt\text{-}f}$=13.7% was then wetted or dried to the target w_f : $w_{1\text{-}f}$=17.6% on the wet side and $w_{2\text{-}f}$=10.6% on the dry side. To attain this purpose, the approach developed by Su et al.

(2021b) was adopted: 1 h of air drying followed by an equilibration time of at least 7 h to lower the water content; conversely, 10 g water was sprayed on the sample followed by the same equilibration time to raise the water content. The wetting or drying procedures ended when the mass of sample increased to that corresponding to $w_{1\text{-f}}$=17.6% or decreased to that corresponding to $w_{2\text{-f}}$=10.6%. The wetting/drying procedures led to a slight swelling/shrinkage of the sample. Accordingly, the measured ρ_d value of the sample slightly decreased or increased (Table 1).

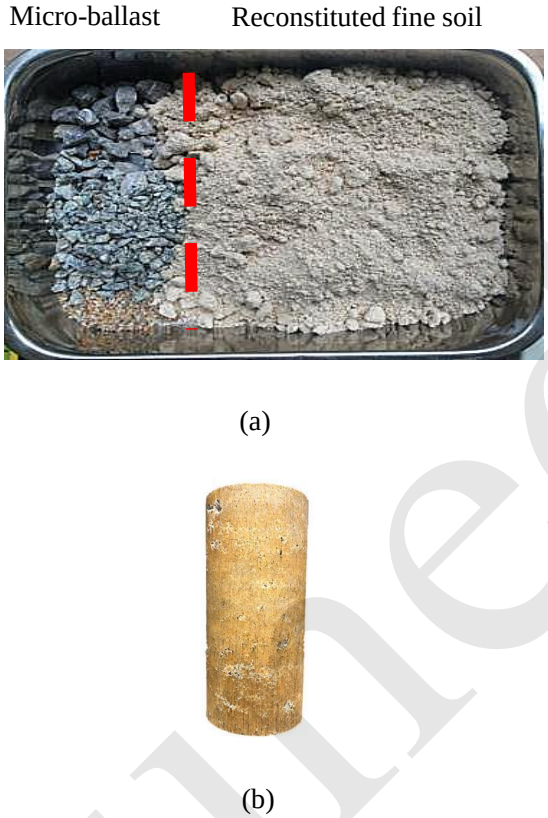

Fig. 2. Overview of (a) reconstituted fines and micro-ballast and (b) as-compacted sample

2.2 Dynamic triaxial tests

The dynamic triaxial testing system (Fig. 3) adopted from Wang et al. (2017) was employed to explore the influences of w_f, f_v and σ_d on the M_r of the soil mixture. The as-compacted cylindrical specimens with three target w_f values (17.6%, 13.7% and 10.6%) and five f_v values (0%, 10%, 20%, 35% and 45%) were tested. A 50 kN hydraulic actuator was mounted, allowing for the application of repeated loading with varying shapes, amplitudes and high-loading cycles. The axial deformation was recorded with a precision of ±0.1 mm. The force sensor at the bottom allows for the precise determination and refined control of the axial force, eliminating the friction between the loading piston and the testing chamber.

A value of confining pressure σ_3=30 kPa was set, which was equivalent to in-situ horizontal stress based on the consideration of interlayer' depth and the train moving load (Trinh et al., 2012). For $w_{1\text{-f}}$=17.6% (S_r=100%), σ_3=30 kPa was employed, followed by overnight consolidation to allow for the dissipation of generated pore water pressure. Afterwards, the specimen was sheared. For $w_{\text{opt-f}}$=13.7% (S_r=78%) and $w_{2\text{-f}}$=10.6% (S_r=60%), the same consolidation time of one night was adopted under σ_3=30 kPa before shearing. All testing procedures were executed in accordance with ASTM D7181-11 (ASTM, 2011). Fig. 4(a) shows an increase in σ_d from 10 to 30 kPa in the loading procedure. These σ_d values ranging from 10 to 30 kPa were selected based on considering axial stress in varying depths of interlayer soil from 250 to 600 mm, which were consistent with Wang et al. (2018b). A number of repeated loadings, N=90,000, was employed for a given σ_d, which was considered to be large enough for the stabilization of a resilient modulus (Gidel et al., 2001; Lamas-López, 2016; Qi et al., 2020a). A loading frequency of 1.78 Hz was set (Fig. 4(b)), equal to that generated under a train speed of 50 km/h in conventional rail tracks. Fig. 4(c) presents a constant stress ratio $\sigma_d/\Delta p$=3 for varying σ_d values, which was a typical in-situ stress path. In these tests, the evolution of deviator stress and axial deformation with time was measured.

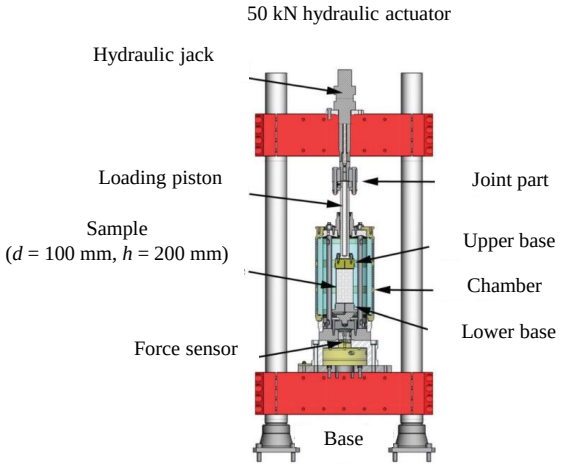

Fig. 3. Schematic view of dynamic triaxial testing system (after Wang et al. 2017)

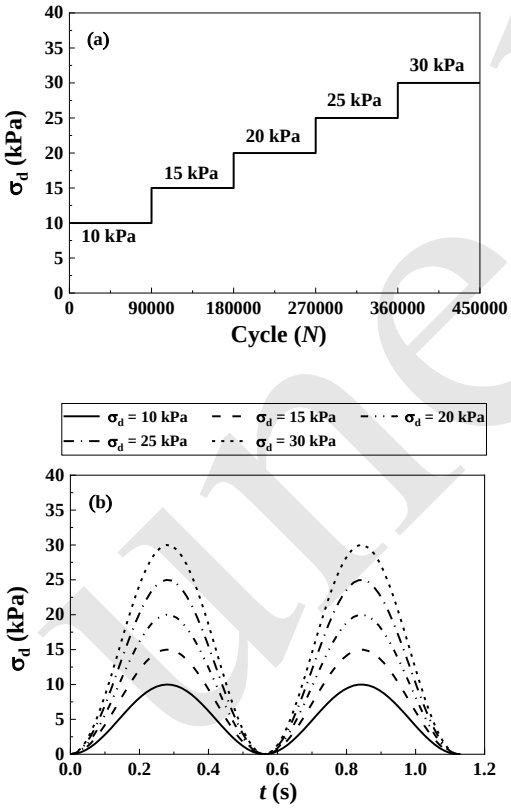

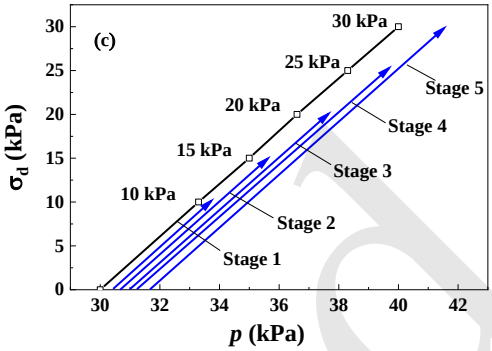

Fig. 4. (a) Multi-stage loading procedure, (b) sine-shaped signals and (c) stress path for varying σ_d

2.3 Mercury intrusion porosimetry tests (MIP)

In this work, MIP tests were conducted, which allowed for observing the microstructure of fines with different w_f values. Three samples at a constant f_v=0% and varying w_f=17.6%, 13.7% and 10.6% were prepared, respectively. The freeze-drying method used by Zhang et al. (2018) was implemented to prepare the fine soil for the MIP test: a piece of fine soil (around 1.5 g) was put into liquid nitrogen under vacuum, followed by storage for at least 24 h in the freeze dryer chamber for sublimation. This method can minimize the microstructure disturbance during dehydration to a large extent, ensuring the quality of MIP results (Delage et al., 2006; Zhang et al. 2018). An Autopore IV 9500 porosimeter was used, allowing the measurement of pore diameter in the 0.006-350 μm range.

3 Experimental results

3.1 Variations in resilient modulus with w_f, f_v and σ_d

Fig. 5 shows the evolution of hysteresis loops with loading cycles N from 0 to 90,000 for the samples at f_v=0%, $w_{1\text{-}f}$=17.6% and σ_d=10 kPa. Under a given hysteresis loop, the axial strain ε_1 consists of permanent strain ε_1^p and resilient strain ε_1^r. The resilient modulus M_r was determined by the ratio of σ_d to ε_1^r in one cycle, which is also the secant slope of the hysteresis loop (for the resilient strain part in Fig.

5). With the progression of N, the size of the hysteresis loop reduced. When the end of the loading stage was reached (e.g., N>10,000), the hysteresis loop became stable. This can be explained as follows: at the beginning of the loading cycles N, the reorientation and rearrangement of particles produced a larger plastic strain $\varepsilon_1^{\mathrm{p}}$. As N increased, more inter-particle contacts developed, initially inducing a smaller plastic strain and finally a purely resilient state. Similar observations were made by Werkmeister et al. (2001, 2004).

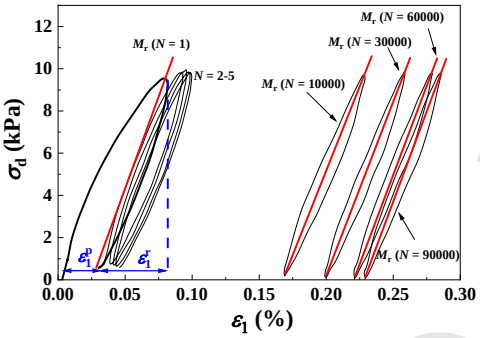

Fig. 5. Plots of typical hysteresis loops for the sample of f_v=0%, $w_{1\text{-f}}$=17.6% and σ_d=10 kPa

Fig. 6(a) shows the evolutions of the end-stage (at N=90,000 for each loading stage) hysteresis loops with σ_d under f_v=0% for $w_{1\text{-f}}$ =17.6%. An increment of σ_d induced an increasing size of the hysteresis loop. Meanwhile, the secant slope of the hysteresis loop decreased as σ_d increased, suggesting that the corresponding M_r decreased. A similar observation was identified for the sample of f_v=0% and $w_{\text{opt-f}}$=13.7%, as shown in Fig. 6(b). By contrast, for the sample of f_v=0% and $w_{2\text{-f}}$ =10.6% in Fig. 6(c), increasing σ_d induced the slight growth of the secant slope and thus a slight increment of M_r accordingly. The decrease of w_f from $w_{1\text{-f}}$=17.6% (Fig. 6(a)) to $w_{2\text{-f}}$=10.6% (Fig. 6(c)) induced a decline of axial strain ε_1 due to the suction effect, which contributed to an increase of M_r.

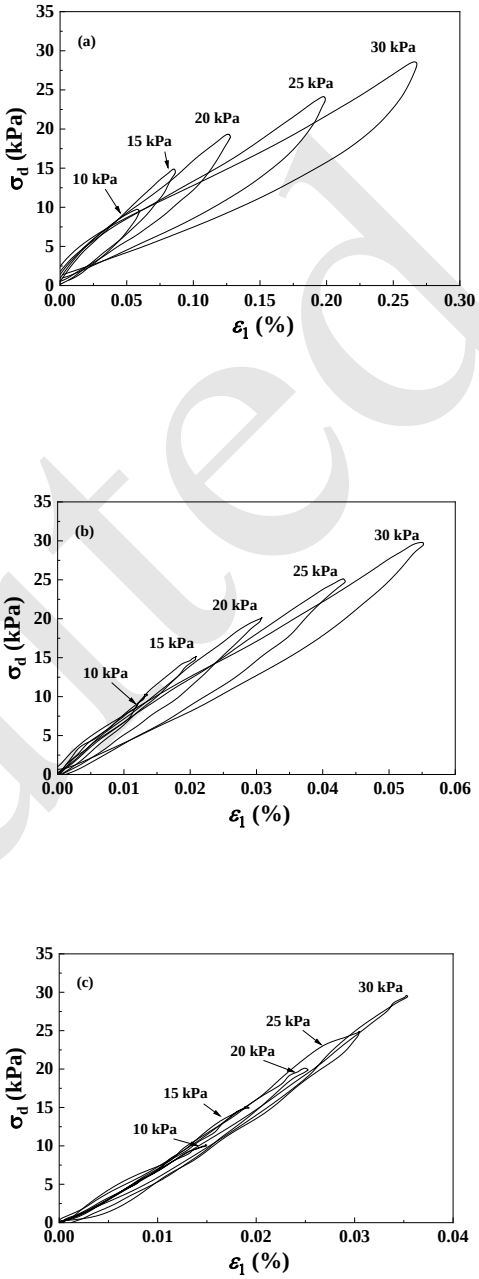

Fig. 6. Plots of end-stage hysteresis loops versus deviator stress σ_d for (a) $w_{1\text{-f}}$=17.6%, (b) $w_{\text{opt-f}}$=13.7% and (c) $w_{2\text{-f}}$=10.6%

Fig. 7(a) shows variations of $\varepsilon_1^{\mathrm{r}}$ with N under f_v=0% for $w_{1\text{-f}}$ =17.6%. At a constant σ_d, the $\varepsilon_1^{\mathrm{r}}$ increased rapidly during the early loading cycles, followed by a gradually decreasing trend until reaching stabilization. This was because the cyclic loading led

to a denser structure with increasing N, and thus a decrease of ε_1^r. When more contacts of particles were developed, the ε_1^r became stable, as shown by Duong et al. (2016). With an increase of σ_d, the ε_1^r increased. Similar observations were identified for the samples with $w_{opt\text{-}f}$=13.7% in Fig. 7(b) and $w_{2\text{-}f}$=10.6% in Fig. 7(c).

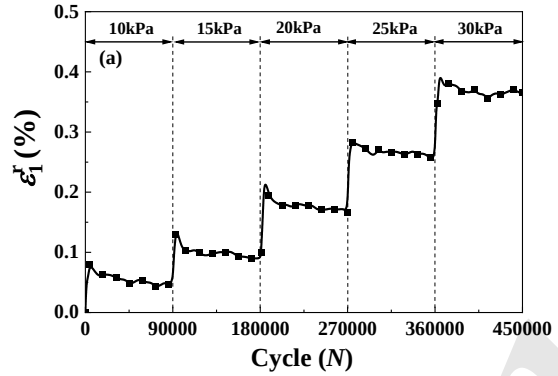

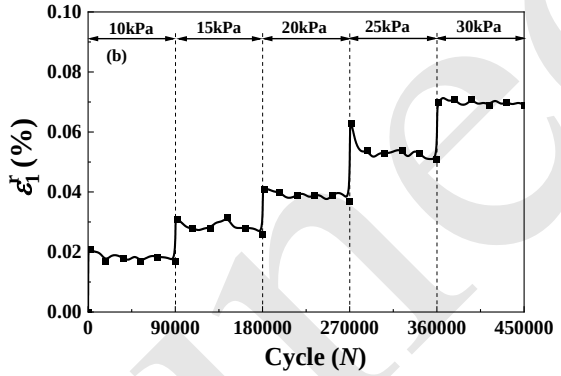

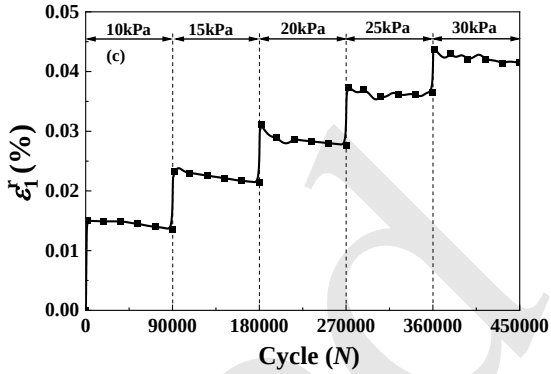

Fig. 7. Plots of resilient strain ε_1^r versus loading cycles N for (a) $w_{1\text{-}f}$=17.6%, (b) $w_{opt\text{-}f}$=13.7% and (c) $w_{2\text{-}f}$=10.6%

Figs. 8(a)–(c) present evolutions of M_r with N under varying f_v and σ_d values for w_f=17.6%, 13.7% and 10.6%, respectively. In Fig. 8(a) ($w_{1\text{-}f}$ =17.6%), under a constant σ_d, M_r increased slightly with the increasing N, which was attributed to the slight decrease of ε_1^r with N in Fig. 7(a). Note that as stated by Werkmeister et al. (2004), under the effect of cyclic loading, the particle rotation and rearrangement occurred. This contributed to a denser structure of soil mixture and thus an increase of its M_r value. The similar observation was made by Duong et al. (2016) on soil mixture with varying f_v=50% and 56%, who found that the M_r of mixture increased with increasing loading cycle. An increment of σ_d induced a decline of M_r. In addition, increasing f_v led to an increase of M_r slightly at f_v=0%–20%, while significantly at f_v=35%–45%. This was attributed to the change of soil fabric: a fine soil supported fabric at f_v=0%–20% and a coarse grain supported fabric at f_v=35%–45%, as evidenced by Wang et al. (2018b). Similar observation were made for the samples with $w_{opt\text{-}f}$=13.7% in Fig. 8(b). Conversely, for the sample with f_v=0% and $w_{2\text{-}f}$ =10.6% in Fig. 8(c), increasing σ_d contributed to an increment of M_r. Note that for the case of $w_{2\text{-}f}$ =10.6%, only the M_r at f_v=0% was presented. That was because the axial strain ε_1 at f_v=10%–45% was beyond the capacity (±0.1 mm) of the axial strain using the testing system. Consequently, the determination of M_r for the samples with $w_{2\text{-}f}$ =10.6% and f_v=10%–45% was not accurate due to the testing limitation, and thus is not depicted in Fig. 8(c).

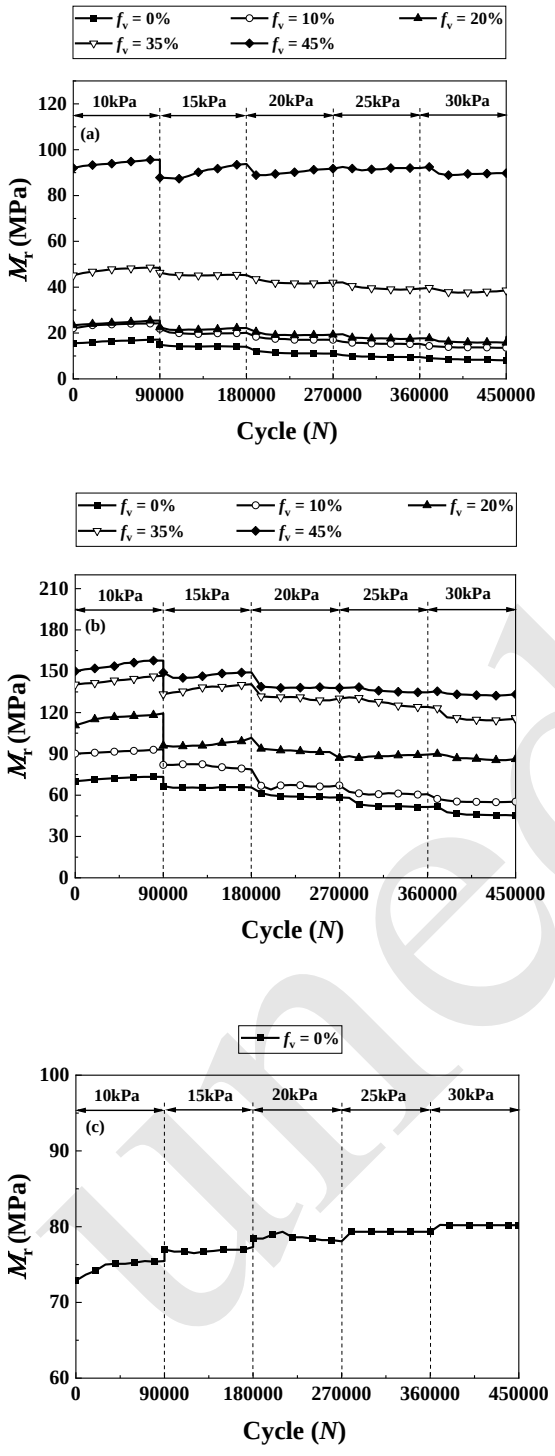

Fig. 8. Plots of resilient modulus M_r versus loading cycles N for (a) $w_{1\text{-f}}$=17.6%, (b) $w_{\text{opt-f}}$=13.7% and (c) $w_{2\text{-f}}$=10.6%

3.2 Variations of pore size distributions with w_f

Fig. 9 presents the pore size distributions (PSDs) of the fine soil for the samples at f_v=0% and w_f=17.6%, 13.7% and 10.6%. Note that, as depicted by Muñoz-Castelblanco et al. (2012), the mercury intruded void ratio of fine soil e_M was determined by the ratio between the volume of intruded mercury V_{Hg} and that of the solid phase V_s. The V_{Hg} was directly obtained from mercury intrusion porosimetry tests, while the V_s is the ratio between the mass of solid m_s and the density of solid ρ_s (ρ_s=2.67 Mg/m^3 in Duong et al. 2013). In Fig. 9(a), the e_M was slightly smaller than the void ratio of fine soil e_f=0.47. In Fig. 9(b), a uni-modal porosity structure was observed for the samples at $w_{1\text{-f}}$ =17.6% and $w_{\text{opt-f}}$=13.7%, with only a micro-pore population identified. However, a bi-modal porosity structure was obtained for the sample with $w_{2\text{-f}}$ =10.6%, with both micro-pore and macro-pore populations characterized. This can be explained below: on the wet side of optimum ($w_{1\text{-f}}$ =17.6%) and at the optimum ($w_{\text{opt-f}}$ =13.7%), a fine matrix fabric was formed due to water hydration, leading to a uni-modal microstructure. As the water content declined, aggregation of the fine soil occurred, as evidenced by Cui and Delage (1996). A fine aggregate fabric was obtained on the dry side of optimum ($w_{2\text{-f}}$ =10.6%), resulting in a bi-modal microstructure. The similar phenomenon was reported by Delage et al. (1996). An increment of w_f from $w_{2\text{-f}}$=10.6% to $w_{\text{opt-f}}$ =13.7% and $w_{1\text{-f}}$=17.6% contributed to the growth of the size of the main micro-pores from 0.17 to 0.29 and 0.59 μm, respectively. This was explained by that increasing w_f induced the swelling of fine soil due to the aforementioned clay fraction (around 30.0%) contained in fine soil (Fig. 1), and thus causing an increase of pore diameter. This was in accordance with the observations of Li and Zhang (2009).

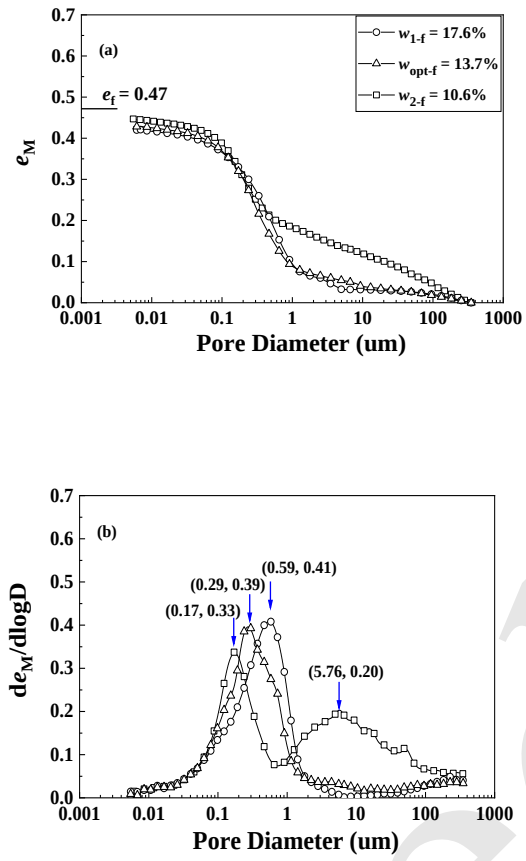

Fig. 9. PSDs of fine soil at f_v=0% and varying water contents: (a) cumulative curves; (b) density function curves

4 Interpretation and discussions

4.1 Combined effects of w_f and σd on M_r

Fig. 10 shows evolutions of the end-stage M_r with w_f under varying σ_d=10–30 kPa for f_v=0%. A threshold water content w_{th}=11.3% was identified. When the w_f was higher than that value, an increment of σ_d induced a reduction of M_r, while a reverse trend was obtained when the w_f was lower. Similar observations were reported by Wang et al. (2017) and Su et al. (2021a) on the same soil mixture with varying f_v=0%–45% under σ_d=50–200 kPa. The w_{th}=12.6%, 11.9%, 11.7%, 12.3% and 13.0% was obtained for f_v=0%, 10%, 20%, 35% and 45%, respectively (Section S2). These values of w_{th} in the present study, Wang et al. (2017) and Su et al. (2021a), were found to be close to the plastic limit of the fine soil w_p=12%. It could thus be inferred that w_p corresponded to the threshold water content w_{th} of the fine/coarse soil mixture. Interestingly, it was found from Figs. 9(a)-(b) that w_p separated the two fabrics of fine soil: a fine matrix fabric at $w_{1\text{-}f}$ =17.6% and $w_{opt\text{-}f}$=13.7% (> w_p =12%) and a fine aggregate fabric at $w_{2\text{-}f}$=10.6% (< w_p =12%). The similar observation was made by Ahmed et al. (1974) on clay and Delage et al. (1996) on silt, who found that w_p was the threshold water content for a fine matrix microstructure and a fine aggregate microstructure. It can be thus inferred that for the fine matrix fabric (w_f>w_p), an increment of σ_d induced a decline of M_r, while for the fine aggregate fabric (w_f<w_p), an increment of σ_d contributed to an increase of M_r.

The M_r–σ_d relationship for these two fabrics was the competing result between soil hardening upon loading and soil rebounding upon unloading. When loading, the growth of σ_d facilitated the compression of fine soil, resulting in an increment of M_r for both fabrics. Conversely, when unloading, the rebounding effect of fine soil led to an increment of ε_1^r, and thus a reduction of M_r. For the fine matrix fabric (w_f>w_p), with respect to its high deformability, the rebounding influence on M_r outweighed the hardening influence. For instance, in Fig. 7(a) ($w_{1\text{-}f}$=17.6%, the fine matrix fabric), an increase of σ_d from 10 to 15 kPa (increase by 50%) led to a large increase of end-stage ε_1^r from 0.05% to 0.10% (increase by 100%). Consequently, an increment of σ_d induced a reduction of M_r for the fine matrix fabric. Conversely, for the fine aggregate fabric (w_f<w_p), the rebounding effect on M_r was secondary compared with the hardening effect based on the consideration of its low deformability. As shown in Fig. 7(c) ($w_{2\text{-}f}$=10.6%), an increase of σ_d from 10 to 15 kPa (increase by 50%) induced a small increase of ε_1^r from 0.014% to 0.020% (increase by 42%). Thus, M_r increased with increasing σ_d for the fine aggregate fabric.

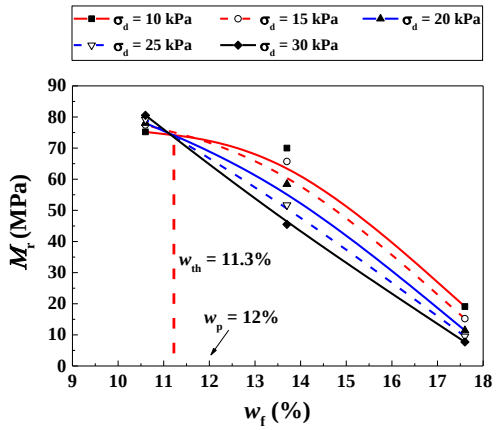

Fig. 10. Plots of end-stage resilient modulus M_r versus water content of fine soil w_f for f_v=0%

4.2 Combined effects of w_f and f_v on M_r

Figs. 11(a)-(b) show that under a given f_v, with increasing deviator stress amplitude σ_d, the decreasing rate of M_r at $w_{opt\text{-}f}$=13.7% was larger than that at w1-f=17.6%. This phenomenon can be explained as follows: according to the findings of Ng et al. (2017), the decrease of w_f from w1-f=17.6% to $w_{opt\text{-}f}$=13.7% induced the shrinkage of soil and a decrease of void ratio (as evidenced by an increase of measured ρ_d in Table 1), which gave rise to an increase of particles contacts. As stated by Werkmeister et al. (2004), the resilient deformation was referred to deformation at particles contacts. In this case, a larger increasing rate of resilient strain ε_1^r was expected at $w_{opt\text{-}f}$=13.7%, and thus a larger decreasing rate of M_r was obtained. Figs. 11(a)-(b) show evolutions of end-stage M_r with σ_d under varying f_v for $w_{1\text{-}f}$=17.6% and $w_{opt\text{-}f}$=13.7% respectively. It was found that the growth of f_v induced an increment of M_r under both saturation ($w_{1\text{-}f}$=17.6%) and unsaturation ($w_{opt\text{-}f}$=13.7%). A comparative work between the present study and Duong et al. (2016) was fulfilled. Duong et al. (2016) explored the M_r of the soil mixture with varying f_v=50.3% and 55.5% for w=12%, 6% and 4% (Figs. 12(a)-(c)). They found that the growth of f_v contributed to an increase of M_r at saturation (w=12%), but a decrease of M_r at unsaturation (w=6% and 4%). The former case (w=12%) is in accordance with the observation in present study (Fig. 11(a)), while the latter cases (w=6% and 4%) are opposed to that observed in present study (Fig. 11(b)).

The combined effects of w_f and f_v on M_r of mixture were linked with the effect of suction ψ. For this work, a constant $\rho_{d\text{-}f}$=1.82 Mg/m^3 of fine soil was kept for varying f_v (Table 1), which led to a constant ψ for a given w (e.g. ψ=739 kPa for a constant $w_{opt\text{-}f}$=13.7% and various f_v values in Wang et al. 2018a, 2018b). This was experimentally examined by Su et al. (2022), who found that the water retention capacity of soil mixture became higher with an increment of $\rho_{d\text{-}f}$, while remained unchanged with an increment of f_v when the $\rho_{d\text{-}f}$ was constant. In this case, the growth of coarse grain content f_v induced an increment of M_r under both saturation and unsaturation (Figs. 11(a)-(b)), which was only due to the reinforcement influence of coarse grains, while being independent of the effect of suction. Conversely, for Duong et al. (2016), given that the ρ_d=2.01 Mg/m^3 of mixture was unchanged, the growth of f_v from 50.3% to 55.5% induced a reduction of $\rho_{d\text{-}f}$ from 1.33 to 1.17 Mg/m^3 (Table 2), and thus a decline of ψ consequently. This was evidenced by Duong et al. (2014), who reported that the growth of f_v from 50.3% to 55.5% induced a decrease of water retention capacity. At saturation (w=12%, Fig. 12(a)), the growth of f_v gave rise to an increment of M_r, which was explained by the only reinforcement effect of coarse grains. By contrast, at unsaturation (w=6% and 4%, Figs. 12(b)-(c)), an increment of f_v contributed to a decline of ψ. While the reinforcement effect of incrementing f_v was less significant than the negative effect of declining ψ, the M_r decreased.

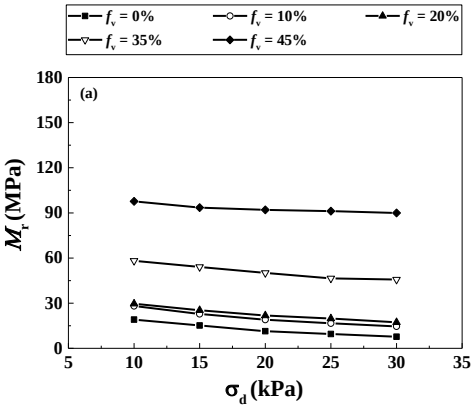

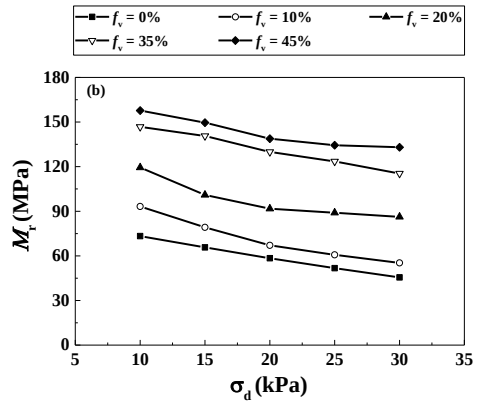

Fig. 11. Plots of end-stage resilient modulus M_r versus deviator stress σ_d for (a) $w_{1\text{-}f}$=17.6%; (b) $w_{opt\text{-}f}$=13.7%

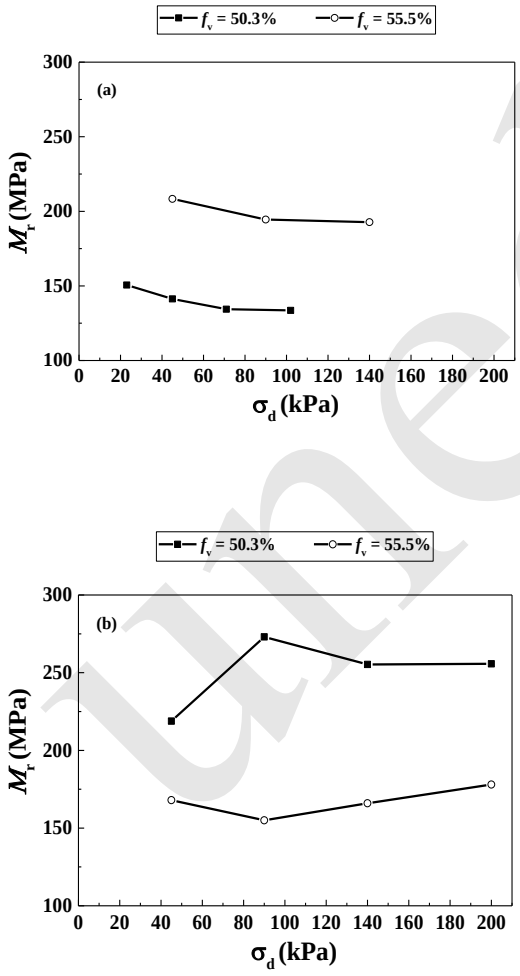

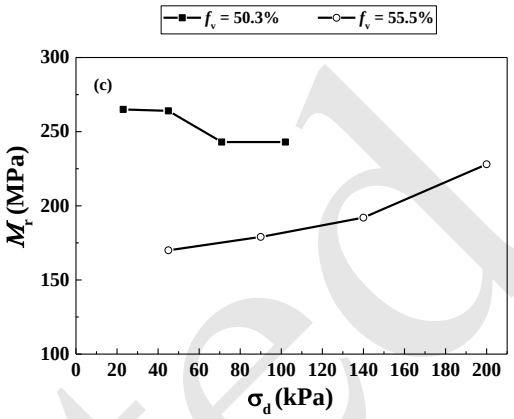

Fig. 12. Plots of end-stage resilient modulus M_r versus deviator stress σ_d for (a) w=12%, (b) w=6% and (c) w=4% (after Duong et al., 2016)

Table 2. Soil properties of Duong et al. (2016)

f_v (%)	w (%)			S_r (%)			ρ_d (Mg/m^3)	$\rho_{d\text{-}f}$ (Mg/m^3)
50.3	4	6	12	32	49	100	2.01	1.33
55.5								1.17

5 Practical implications of present study

From a practical point of view, with increasing train moving loads, the M_r of the interlayer soil increases at low water content (smaller than the plastic limit of fine soil fraction w_p) but decreases at high water content (larger than the w_p). This suggests that a drainage system in the railway substructure is required, for ensuring the normal performance of interlayer soil, especially under varying train moving loads. Otherwise, a decrease in the stiffness of interlayer soil is expected.

6 Conclusions

This study is to address the relationship between the M_r of soil mixture and the microstructure of fines. MIP tests were fulfilled for observing the fabric of fine soil at different w_f, while dynamic triaxial tests

with varying σ_d were carried out for the determination of M_r of soil mixture with various w_f and f_v. From these tests, the following conclusions were obtained.

1) For the fine matrix fabric ($w_f>w_p$), the growth of σ_d contributed to a decline of M_r of soil mixture, while for the fine aggregate fabric ($w_f<w_p$), the growth of σ_d gave rise to an increment of M_r.
2) The M_r–σ_d relationship for the two fabrics was determined by the competing result between the soil hardening upon loading and the soil rebounding upon unloading. For the fine matrix fabric ($w_f>w_p$), with respect to its high deformability, the rebounding influence on M_r outweighed the hardening influence. Conversely, for the fine aggregate fabric ($w_f<w_p$), the rebounding effect on M_r was secondary compared with the hardening effect based on the consideration of its low deformability.
3) The combined influences of w_f and f_v on M_r were linked with the influence of suction. Under saturation, the increase of M_r with increasing f_v was explained by the reinforcement influence of coarse grains. Under unsaturation, when the reinforcement influence of incrementing f_v was less significant than the negative influence of decreasing ψ, the M_r decreased.

Acknowledgments

The research was supported by National Natural Science Foundation of China (Nos. 52208347 and 52208348), Jiangxi Provincial Natural Science Foundation (Nos. 20224BAB214063, 20224BAB214064 and 20232BAB204083) and China Postdoctoral Science Foundation (No. 2023M731436).

Author contributions (refer to https://www.casrai.org/credit.html)

Junyi Duan designed the research. Yue Zhang processed the corresponding data. Yu Su wrote the first draft of the manuscript. Jianglin Gao and Zhongzheng Wang helped to organize the manuscript. Da Liu, Bo Han and Wenzhe Zhu revised and edited the final version.

Conflict of interest

Yu Su, Yue Zhang, Junyi Duan, Jianglin Gao, Zhongzheng Wang, Da Liu, Bo Han, Wenzhe Zhu declare that they have no conflict of interest.

References

Cao YL, 2003. Study on the Methodology and Technology of Robust Tolerance Design for Manufacture. PhD Thesis, *Zhejiang University*, Hangzhou, China (in Chinese).

Cavalier T, Lehtihet A, 2000. A comparative evaluation of sequential set point adjustment procedures for tolerance control. *International Journal of Production Research*, 38(8):1769-1777. https://doi.org/10.1080/002075400188582

Etesami FA, 1993. A mathematical model for geometric tolerances. *Journal of Mechanical Design*, 115(1):81-86. https://doi.org/10.1115/1.2919329

Gorini S, Quirini M, Menciassi A, et al., 2006. A novel SMA-based actuator for a legged endoscopic capsule. *First IEEE/RAS-EMBS International Conference on Biomedical Robotics and Biomechatronics*, p.443-449. https://doi.org/10.1109/BIOROB.2006.1639128

Tanner NA, Wait JR, Farrar CR, et al., 2003. Structural health monitoring using modular wireless sensors. *Journal of Intelligent Material Systems and Structures*, 14(1):43-56. https://doi.org/10.1177/1045389X03014001005

Wu ZT, Yang JX, 1999. Computer Aided Tolerance Optimization Design. *Zhejiang University Press*, Hangzhou, China, p.85-124 (in Chinese).

Ahmed S, Lovell CW, Diamond S, 1974. Pore sizes and strength of compacted clay. *Journal of the Geotechnical Engineering Division*, 100(4):407-425. https://doi.org/10.1061/AJGEB6.0000035

ASTM (American Society for Testing and Materials), 2011. Method for Consolidated Drained Triaxial Compression Test for Soils, *ASTM D7181-11*. *Standards of USA*. https://doi.org/10.1520/D7181-11

Anagnostopoulos CA, Chrysanidis T, Anagnostopoulou M, 2020. Experimental data of cement grouting in coarse soils with different superplasticisers. *Data in Brief*, 30, 105612.

Alamanis N, Lokkas P, Chrysanidis T, et al., 2021. Assessment principles for the mechanical behavior of clay soils. *WSEAS Transactions on Applied and Theoretical Mechanics*, 16, 47-61.

Bian XC, Wan ZB, Zhao C, et al., 2022. Mud pumping in the roadbed of ballastless high-speed railway. *Géotechnique*, 1-15. https://doi.org/10.1680/jgeot.21.00135

Charles WWN, Lu BW, Ni JJ, et al., 2019. Effects of vegetation type on water infiltration in a three-layer cover system using recycled concrete. *Journal of Zhejiang University-SCIENCE A (Applied Physics & Engineering)*, 20(1):1-9. https://doi.org/10.1631/jzus.A1800373

Cui YJ, Delage P, 1996. Yielding and plastic behaviour of an unsaturated compacted silt. *Géotechnique*, 46(2):291-311. https://doi.org/10.1680/geot.1996.46.2.291

Delage P, Audiguier M, Cui YJ, et al., 1996. Microstructure of a compacted silt. *Canadian Geotechnical Journal*, 33(1):150-158. https://doi.org/10.1139/t96-030

Delage P, Marcial D, Cui YJ, et al., 2006. Ageing effects in a compacted bentonite: a microstructure approach. *Géotechnique*, 56(5):291-304.

https://doi.org/10.1680/geot.2006.56.5.291

Duong TV, Tang AM, Cui YJ, et al., 2013. Effects of fines and water contents on the mechanical behavior of interlayer soil in ancient railway sub-structure. *Soils and Foundations*, 53(6):868-878. https://doi.org/10.1016/j.sandf.2013.10.006

Duong TV, Cui YJ, Tang AM, et al., 2014. Effect of fine particles on the hydraulic behavior of interlayer soil in railway substructure. *Canadian Geotechnical Journal*, 51(7):735-746. https://doi.org/10.1139/cgj-2013-0170

Duong TV, Cui YJ, Tang AM, et al., 2016. Effects of water and fines contents on the resilient modulus of the interlayer soil of railway substructure. *Acta Geotechnica*, 11(1):51-59. https://doi.org/10.1007/s11440-014-0341-0

Gidel G, Hornych P, Chauvin JJ, et al., 2001. A new approach for investigating the permanent deformation behavior of unbound granular material using the repeated load triaxial apparatus. *Bulletin des laboratoires des Ponts et Chaussées*, (233):5-21.

Hu J, Bian XC, 2022. Analysis of dynamic stresses in ballasted railway track due to train passages at high speeds. *Journal of Zhejiang University-SCIENCE A (Applied Physics & Engineering)*, 23(6):443-457. https://doi.org/10.1631/jzus.A2100305

Indraratna B, Ngo T, Ferreira FB, et al., 2021. Large-scale testing facility for heavy haul track. *Transportation Geotechnics*, 28:100517. https://doi.org/10.1016/j.trgeo.2021.100517

Lamas-López F, 2016. Field and Laboratory Investigation on the Dynamic Behaviour of Conventional Railway Track-Bed Materials in the Context of Traffic Upgrade. PhD Thesis, *Ecole Nationale des Ponts et Chaussées, Université Paris-Est*.

Lekarp F, Isacsson U, Dawson A, 2000. State of the art. I: resilient response of unbound aggregates. *Journal of Transportation Engineering*, 126(1):66-75. https://doi.org/10.1061/(ASCE)0733-947X(2000)126:1(66)

Li X, Zhang LM, 2009. Characterization of dual-structure pore-size distribution of soil. *Canadian Geotechnical Journal*, 46(2):129-141. https://doi.org/10.1139/T08-110

Lokkas, P. , Chouliaras, I. , Chrisanidis, T. , Christodoulou, D. , & Paschalis, E. . 2021. *Historical background and evolution of soil mechanics*.

Muñoz-Castelblanco JA, Pereira JM, Delage P, et al., 2012. The water retention properties of a natural unsaturated loess from northern France. *Géotechnique*, 62(2):95-106. https://doi.org/10.1680/geot.9.P.084

Ng CWW, Zhou C, Yuan Q, et al., 2013. Resilient modulus of unsaturated subgrade soil: experimental and theoretical investigations. *Canadian Geotechnical Journal*, 50(2):223-232. https://doi.org/10.1139/cgj-2012-0052

Ng, C. W. W., Baghbanrezvan, S., Sadeghi, H., Zhou, C., & Jafarzadeh, F. (2017). Effect of specimen preparation techniques on dynamic properties of unsaturated fine-grained soil at high suctions. *Canadian Geotechnical Journal*, 54(9), 1310-1319.

Qi S, Cui YJ, Dupla JC, et al., 2020a. Investigation of the parallel gradation method based on the response of track-bed materials under cyclic loadings. *Transportation Geotechnics*, 24:100360. https://doi.org/10.1016/j.trgeo.2020.100360

Qi S, Cui YJ, Chen RP, et al., 2020b. Influence of grain size distribution of inclusions on the mechanical behaviours of track-bed materials. *Géotechnique*, 70(3):238-247. https://doi.org/10.1680/jgeot.18.P.047

Su, Y., Cui, Y. J., Dupla, J. C., & Canou, J. 2020. Investigation of the effect of water content on the mechanical behavior of track-bed materials under various coarse grain contents. *Construction and Building Materials*, 263, 120206

Su Y, Cui YJ, Dupla JC, et al., 2021a. Effect of water content on resilient modulus and damping ratio of fine/coarse soil mixtures with varying coarse grain contents. *Transportation Geotechnics*, 26:100452. https://doi.org/10.1016/j.trgeo.2020.100452

Su Y, Cui YJ, Dupla JC, et al., 2021b. Developing a sample preparation approach to study the mechanical behavior of unsaturated fine/coarse soil mixture. *Geotechnical Testing Journal*, 44(4):20190450. https://doi.org/10.1520/GTJ20190450

Su Y, Cui YJ, Dupla JC, et al., 2022. Soil-water retention behaviour of fine/coarse soil mixture with varying coarse grain contents and fine soil dry densities. *Canadian Geotechnical Journal*, 59(2):291-299. https://doi.org/10.1139/cgj-2021-0054

Sun QD, Indraratna B, Nimbalkar S, 2016. Deformation and degradation mechanisms of railway ballast under high frequency cyclic loading. *Journal of Geotechnical and Geoenvironmental Engineering*, 142(1):04015056. https://doi.org/10.1061/(ASCE)GT.1943-5606.0001375

Sun Y, Nimbalkar S, Chen C, 2018. Grading and frequency dependence of the resilient modulus of ballast. *Géotechnique Letters*, 8(4):305-309. https://doi.org/10.1680/jgele.18.00084

Trinh VN, 2011. Comportement Hydromécanique de Matériaux Constitutifs de Plateformes Ferroviaires Anciennes. *PhD Thesis, Université Paris-Est*, Paris, France.

Trinh VN, Tang AM, Cui YJ, et al., 2012. Mechanical characterisation of the fouled ballast in ancient railway track substructure by large-scale triaxial tests. *Soils and Foundations*, 52(3):511-523. https://doi.org/10.1016/j.sandf.2012.05.009

Van Genuchten, M. T. 1980. A closed-form equation for predicting the hydraulic conductivity of unsaturated soils. *Soil science society of America journal*, 44(5), 892-898.

Wan ZB, Bian XC, Li SH, et al., 2020. Remediation of mud pumping in ballastless high-speed railway using polyurethane chemical injection. *Construction and Building Materials*, 259:120401. https://doi.org/10.1016/j.conbuildmat.2020.120401

Wang HL, Cui YJ, Lamas-Lopez F, et al., 2017. Effects of inclusion contents on resilient modulus and damping ratio of unsaturated track-bed materials. *Canadian Geotechnical Journal*, 54(12):1672-1681. https://doi.org/10.1139/cgj-2016-0673

Wang HL, Cui YJ, Lamas-Lopez F, et al., 2018a. Investigation on the mechanical behavior of track-bed materials at various contents of coarse grains. *Construction and Building Materials*, 164:228-237. https://doi.org/10.1016/j.conbuildmat.2017.12.209

Wang HL, Cui YJ, Lamas-Lopez F, et al., 2018b. Permanent deformation of track-bed materials at various inclusion contents under large number of loading cycles. *Journal of Geotechnical and Geoenvironmental Engineering*, 144(8):04018044. https://doi.org/10.1061/(ASCE)GT.1943-5606.0001911

Wang HL, Chen RP, Cheng W, et al., 2019. Full-scale model study on variations of soil stress in geosynthetic-reinforced pile-supported track bed with water level change and cyclic loading. *Canadian Geotechnical Journal*, 56(1):60-68. https://doi.org/10.1139/cgj-2017-0689

Werkmeister S, Dawson AR, Wellner F, 2001. Permanent deformation behavior of granular materials and the shakedown concept. Transportation Research Record: *Journal of the Transportation Research Board*, 1757(1):75-81. https://doi.org/10.3141/1757-09

Werkmeister S, Dawson AR, Wellner F, 2004. Pavement design model for unbound granular materials. *Journal of Transportation Engineering*, 130(5):665-674. https://doi.org/10.1061/(ASCE)0733-947X(2004)130:5(665)

Yang SR, Lin HD, Kung JHS, et al., 2008. Suction-controlled laboratory test on resilient modulus of unsaturated compacted subgrade soils. *Journal of Geotechnical and Geoenvironmental Engineering*, 134(9):1375-1384. https://doi.org/10.1061/(ASCE)1090-0241(2008)134:9(1375)

Zhang F, Cui YJ, Zeng LL, et al., 2018. Effect of degree of saturation on the unconfined compressive strength of natural stiff clays with consideration of air entry value. *Engineering Geology*, 237:140-148. https://doi.org/10.1016/j.enggeo.2018.02.013

Zheng H, Zhang C, Yang Z, 2020. A local radial basis function collocation method for band structure computation of 3D phononic crystals. *Applied Mathematical Modelling*, 77:1954-1964. https://doi.org/10.1016/j.apm.2019.09.006

Electronic supplementary materials

Section S1 and S2

中文概要：

题　目： 列车荷载-含水量-粗颗粒含量共同作用下混合物回弹模量的演化机制研究

作　者： 粟雨[1,2]，张悦[1]，段君义[1]，高江林[2]，王中正[3]，刘达[2]，韩波[1]，朱文哲[1]

机　构： [1]南昌大学工程建设学院，江西 南昌 330031；[2]江西省水利科学院江西省水工安全工程技术研究中心，江西 南昌 330029；[3]昆士兰科技大学工程学院，澳大利亚 QLD 4001

目　的： 由于列车长期荷载作用，道砟嵌入基床表层细粒土，形成铁路路基夹层。随着荷载幅值、道砟含量和含水量的变化，夹层中粗-细粒混合物的回弹模量发生改变，严重影响整个路基的正常服役性能。本文旨在研究荷载幅值 σ_d、粗颗粒含量 f_v 和含水量 w_f 共同作用下混合物回弹模量 M_r 的演化规律，和在此过程中细粒土微观结构的变化，并揭示两者之间的内在关联。

创新点： 揭示荷载幅值 σ_d 和含水量 w_f 对混合物回弹模量的耦合作用，并解释这种耦合作用产生的微观机理。

方　法： 1. 基于动三轴试验，揭示荷载幅值 σ_d、粗颗粒含量 f_v 和含水量 w_f 共同作用下混合物回弹模量的演化规律；通过压汞试验，揭示不同含水量下细粒土微观结构的变化。

结　论： 荷载幅值 σ_d 和含水量 w_f 对混合物回弹模量 M_r 存在耦合作用——当 $w_f>w_p$（塑限），随着 σ_d 增加，M_r 降低；当 $w_f<w_p$，随着 σ_d 增加，M_r 增加。这种耦合作用的产生可归因于细粒土微观结构变化：当 $w_f<w_p$ 时，细粒土为凝块状的团粒结构，具有低压缩性，随着 σ_d 增大，M_r 增大；当 $w_f>w_p$ 时，随着含水量增加，团粒结构逐渐分解、解体，可压缩性增加，因而出现相 反的情况。

关键词： 回弹模量；混合物；动三轴；压汞试验；含水量；粗颗粒含量